Geochimica et Cosmochimica Acta, Vol. 69, No. 22, pp. 5187–5201, 2005

0016-7037/05 $30.00 + .00

doi:10.1016/j.gca.2005.05.020

Geochemistry of unsaturated soil systems: Aqueous speciation and solubility of minerals and gases in capillary solutions

ARNAULT LASSIN,[1,*] MOHAMED AZAROUAL,[1] and LIONEL MERCURY[2]

[1]BRGM, 3 av. C. Guillemin, BP 6009, 45060 Orléans, France
[2]UMR-CNRS 8148 "IDES," Université Paris-Sud, bat. 504, 91405 Orsay, France

(*Received December* 20, 2004; *accepted in revised form May* 31, 2005)

Abstract—It has been shown that the capillary state of aqueous solutions in the unsaturated zone (UZ) modifies chemical equilibria due to the decreasing capillary pressure of the whole system (isobaric scenario) or of the aqueous phase only (anisobaric scenario). Meanwhile, the role of salinity in capillary solutions has not been explicitly taken into account up to now, at least not in a manner independent to capillarity. A consistent way to do so is considered in this paper by calculating activity coefficients as a function of capillary pressure through the extrapolation of the Davies model. The integrated approach thus defined is applied to the interpretation of some laboratory experiments (taken from the literature) carried out under different capillary conditions. Calculations and measurements of the boehmite $\leftrightarrow$ bayerite hydration equilibrium in an atmosphere of varying humidity agree very satisfactorily if the anisobaric scenario is selected. The solubility of reactive gases O_2 and CO_2 is found to increase in the pore water when the relative humidity decreases. Consequently, and in agreement with experimental measurements, the extent of the pyrite oxidation depends on the relative humidity. The proposed model refines the manner with which chemical equilibria and mineralogical assemblies may be interpreted. In particular, the different scenarios that may be envisioned (isobaric, anisobaric and dual) are considered in the light of the possible modes of precipitation of the minerals (precipitation within the capillary solution, epitaxial type precipitation). Finally, it should be noted that the geochemical approach proposed here for the UZ fully ties in with and conforms to the methods used in the water-saturated zone (SZ).

1. INTRODUCTION

Thermodynamic and kinetic approaches are widely used in groundwater and surface water studies to quantify/predict the intensive/extensive levels of the acting physical and chemical processes. Geochemical calculation codes (Phreeqc, EQ3/6, etc.) make these approaches easier and more powerful so that they are applied to a very wide range of hydrogeochemical systems by the scientific community.

The basic concepts of water-rock interactions were developed for the water-saturated domain, and have been extended towards the unsaturated zone (UZ), in general by some parameters which correct for the water volumetric saturation in such media. However, the whole theoretical SZ frame is then used, implicitly assuming that the chemical equilibria are not modified by the capillary nature of the UZ solutions.

Yet, the chemical consequences of unsaturated conditions are well known, in particular in studies of clay hydration isotherms (Barshad, 1955), of soil geochemistry (Tardy, 1982; Bourrié et al., 1983; Tardy and Nahon, 1985; Trolard and Tardy, 1987, 1989; Tardy and Novikoff, 1988; Zilberbrand, 1997, 1999; Mercury and Tardy, 1997a,b, 2001, 2004; Mercury et al., 2003), of paleoclimatic studies using noble gases (Mercury et al., 2004), of nuclear waste storage in unsaturated rocks (Bruton and Viani, 1992), and of conservation of buildings (Benavente et al., 2004).

All these studies share a common theoretical background related to the influence of the chemical potential of capillary water on the solid-aqueous solution interactions, but use more or less different methods. The most recent method (Mercury and Tardy, 2001, 2004; Mercury et al., 2003) relies on the calculation of the effect of the internal pressure of capillary water on its thermodynamic and electrostatic properties. This method allows to extend, in a *continuum,* the thermodynamic description of the geochemistry from the SZ up to the UZ. This continuum is essentially provided by using the same pressure parameter to describe the water state in all configurations.

The objective of the present article is to complete the capillary pressure approach tested up to now on dilute solutions, by addressing the role of salinity, i.e., of the osmotic contribution of the interactions. This is done by calculating the activity coefficients of the aqueous (capillary) solutes, as a function of both (but in a distinct manner) the capillary pressure of the solution and its salinity. The overall model thus becomes more suited to the resolution of a number of geochemical problems and is applied in this paper to some laboratory data reported in the literature.

This article is set out in the following manner. In a first section, the fundamental physical and chemical aspects of the UZ are presented. In a second section, the approach is applied to real, simple case studies. The agreement between calculations and observations is then discussed, underlining by the way the physical meaning of the theoretical concepts of the proposed approach. Finally, the entire reasoning is summarized and some perspectives are provided.

2. THEORY

The activity of water (a_w) is the classical parameter used to describe the thermodynamic equilibrium between an under-

* Author to whom correspondence should be addressed (a.lassin@brgm.fr).

saturated atmosphere ($p/p_0 < 1$) and liquid water, whatever the origin of this equilibrium: capillary ($P_{\text{water}} < 0.1$ MPa), osmotic (ionic strength $I > 10^{-7}$ eq · kgw^{-1}) or interfacial (surface tension $\sigma_{\text{film-vapor}} \neq \sigma_{\text{bulk-vapor}}$). It is defined as the ratio between the partial pressure of water vapor in the ambient air, p, and the partial pressure of saturated vapor at the temperature T of the studied system, p_0, i.e., $a_w = p/p_0$. According to this definition, the activity of water is related to the relative humidity of the air (RH) by:

$$a_w = RH/100 = p/p_0\,. \tag{1}$$

Leaving aside wetting phenomena, one may therefore state that a concentrated solution ($P_{\text{water}} \geq 0.1$ MPa, $I > 10^{-7}$ eq · kgw^{-1}) and a pure capillary water ($P_{\text{water}} < 0.1$ MPa, $I \sim 10^{-7}$ eq · kgw^{-1}) may be indiscernible in terms of chemical potential. However, at equivalent RH, the former depends on the nature and the concentration of the dissolved solutes, while the latter depends on the size of the pores.

The capillary state of liquid water in the UZ is assumed through its decreasing internal pressure. All of the properties of water and of the solutes (one assumes $P_{\text{solutes}} = P_{\text{water}}$) have to be corrected accordingly. In addition, for saline solutions, activity coefficients must be taken into account, as well as the variation of these coefficients as a function of ionic strength and pressure of the capillary solution. This implies that capillary water is pure water ($a_w = 1$) at its standard state (Mercury and Tardy, 2001). Only salinity makes the activity of water different from unity, and the effect of capillarity is assumed through the mechanical energy term (VdP) of the equation of state. This framework is strictly similar to that used for the saturated zone (SZ) (Helgeson et al., 1981).

Strictly speaking, the calculation of the internal pressure of water in the capillary solution at equilibrium with a given relative humidity must take the salinity of the solution into account. In other words, the following relation should replace Eqn. 1:

$$\mathrm{R}T\ln\frac{RH}{100} = \mathrm{R}T\ln\frac{P_{\text{water}}}{p_0} = \mathrm{R}T\ln a_w + \int_{P_r}^{p} V_w \cdot dP\,, \tag{2}$$

where a_w is the activity of water due to the effects of the salinity of the solution and V_w is the molar volume of pure water.

By way of comparison, Bruton and Viani (1992) based their simulation of the capillarity on the apparent equivalence between the osmotic and capillary effects, by introducing into their model solution a noncharged and nonreactive compound, which was absent from the actual solutions. That allowed them to artificially reduce the water activity (according to $\log a_w = 1 - 0.018\ \Sigma m_i$, where m_i is the molality of compound i) in order to fit the chemical potential of water actually due to both the capillary (UZ) and the osmotic (salinity) conditions. On the contrary, Eqn. 2 allows a clear distinction between the capillary and osmotic components, consistent with the approach of soil physicists, who break down the total potential of water in soil into a matrix term (i.e., capillary) and an osmotic term (e.g., Hillel, 1998).

2.1. Internal Pressure of Capillary Water (Case of Pure Water, $a_w = 1$)

Numerous studies (Mercury and Tardy, 2001, 2004, and references therein) have highlighted the actual situations wherein the stretched (or capillary) liquid water is encountered. In the present study, the main focus will be the suspended water of the UZ where localized portions of capillary water persist above air.

The two main capillary laws, which are very useful in considering the physics and chemistry of the UZ, are the Young-Laplace and Kelvin laws. The former links the curve r (m) of a "humid air"–water interface to the pressure difference ΔP (Pa) between these two phases. For a spherical interface, the Young-Laplace relationship is expressed as:

$$\Delta P = P_{\text{water}} - P_{\text{air}} = \frac{2\sigma}{r}. \tag{3}$$

where σ (J · m^{-2}) is the interfacial tension, P_{water} is the pressure in the pure capillary water ($a_w = 1$) and P_{air} is the total pressure of the gaseous phase containing the partial pressure of water vapor p ($\leq p_0$). By convention, r is negative for a concave interface towards the air (capillary meniscus).

The Kelvin law provides the radius r_K of the "humid air"–water interfacial meniscus in equilibrium with the relative humidity of the air RH ($=100 \times p/p_0$). This radius, known as the Kelvin radius, is the maximum radius of the pores within which capillary condensation can take place, below which the pores are filled with water. For a cylindrical pore, the Kelvin law may be expressed as:

$$\frac{\sigma}{r_K} = \frac{\rho \mathrm{R}T}{M_w N_a}\ln\frac{p}{p_0}, \tag{4}$$

where ρ is the density of the pure water (g·m^{-3}), R = 8.314 J · mol^{-1} · K^{-1} is the ideal gas constant; T is the absolute temperature (K); $M_w = 18.015$ g · mol^{-1} is the molar mass of water; and $N_a = 6.023 \times 10^{23}$ mol^{-1} is Avogadro's number.

According to the model known as the BJH model (Barrett et al., 1951), the thickness of the multilayered water adsorbed at the surface of the solid must be added to the Kelvin radius in order to deduce the maximum size of the pores filled with water at a given relative humidity. Then, the Kelvin radius (Eqn. 4) actually is the radius of the curved liquid interface. For a more in-depth discussion about calculated meniscus and pore radii, the interested reader is referred to Mercury and Tardy (2004).

Then, assuming that at the thermodynamic equilibrium (physical and chemical) one has $r = r_K$, the combination of Eqns. 3 and 4 provides the internal pressure of the pure capillary water at equilibrium with an atmosphere of fixed relative humidity:

$$P_{\text{water}} = \frac{2\rho \mathrm{R}T}{M_w N_a}\ln\frac{p}{p_0} + P_{\text{air}}. \tag{5}$$

This expression, graphically represented in Figure 1, indicates that, for a relative humidity RH less than 100% (or $p/p_O < 1$, Eqn. 2), the internal pressure of the pure capillary water P_w is subatmospheric. In parallel, Eqn. 4 results in a very rapid decrease in the Kelvin radius (down to around 10 nm) when the

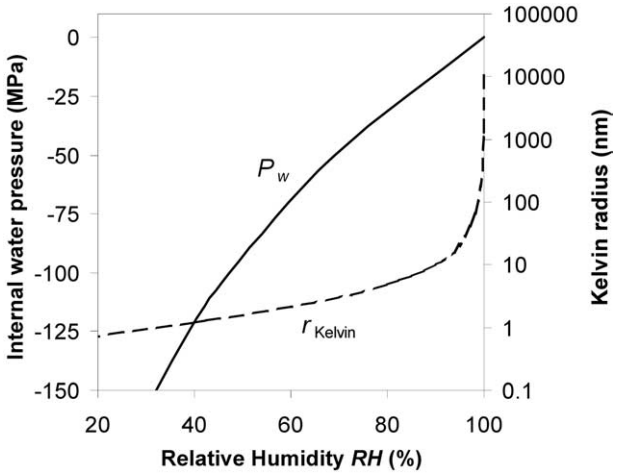

Fig. 1. Internal pressure of capillary water as a function of relative humidity (according to Eqn. 5) and corresponding Kelvin radius (according to Eqn. 4) at $T = 25°C$.

relative humidity decreases from 100 to 95%. Below 95% *RH*, the decreasing slope is lowered when the relative humidity continues to decrease (Fig. 1).

2.2. Thermodynamic Properties of Capillary Water

The temperature and pressure conditions at which the stretched liquid water has been observed are in the metastability domain below the saturation curve but above the spinodal curve (Fig. 2), both depicted by the Wagner and Pruss' equation of state (Wagner and Pruss, 2002). The liquid-vapor spinodal curve is, for each temperature, the locus for which the water pressure (P) attains a minimum value compared to the density (ρ), that is,

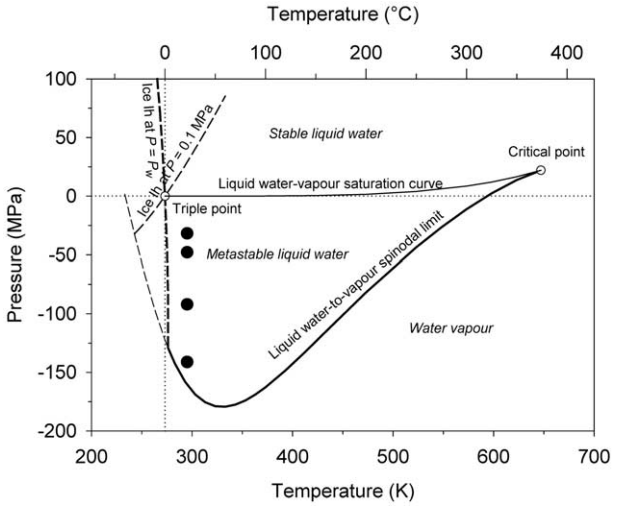

Fig. 2. Water stability diagram, modified from Mercury and Tardy (2001); (P,T) localization of the metastability zone corresponding to the existence domain of capillary water. Full circles correspond to the experimental plots that were used in the pyrite oxidation study in humid atmosphere performed by Borek (1994), cf. section 3.2.

$$\left(\frac{\partial P}{\partial \rho}\right)_T = 0 \quad \text{and} \quad \left(\frac{\partial^2 P}{\partial \rho^2}\right)_T < 0.$$

In other terms, the spinodal is the intrinsic limit of metastability of liquid water. Beyond this limit, liquid water (that which obeys the equation of state) is unstable and cavitates spontaneously (homogeneous nucleation).

The thermodynamic properties of pure capillary water are calculated from the equation of state which, from the Helmholtz free energy A as a function of the density ρ and the temperature T, derives the entire set of properties: the standard Gibbs free energy and enthalpy of formation of water from elements (ΔG_f°, ΔH_f°, respectively), the entropy of the third law of thermodynamics ($S°$;, calculated by integration of the function $C_P(T)$), the heat capacity at constant pressure (C_P), the isobaric expansivity (α), the isothermic compressibility (β) and the pressure (P). The dielectric constant (ε) of water is calculated as a function of P,T conditions, according to the equation developed by Fernández et al. (1997). These formalisms are recommended by the International Association for the Properties of Water and Steam (IAPWS) and are consistent with each other.

This approach relies on the explicit assumption that these equations characterizing pure water extend in the metastability domain, i.e., the thermodynamic and electrostatic properties of liquid water evolve continuously down to the spinodal limit. The internal pressure of water in the UZ (P_w) thus allows to calculate the standard chemical potential of liquid water (Mercury and Tardy, 2001) with a unified formalism in both the saturated and unsaturated zones, which illustrates the notion of thermodynamic continuum.

2.3. Thermodynamic Properties of Aqueous Species

The dielectric constant of water, its partial derivatives, the isobaric expansivity,

$$\alpha = -\frac{1}{\rho}\left(\frac{\partial \rho}{\partial T}\right)_P,$$

and the isothermic compressibility,

$$\beta = \frac{1}{\rho}\left(\frac{\partial \rho}{\partial P}\right)_T$$

are used to calculate the Born functions. These functions play a particularly important role in the Helgeson-Kirkham-Flowers or HKF model (Helgeson et al., 1981), developed for calculating the thermodynamic properties of aqueous species (Johnson et al., 1992) over a wide range of pressures and temperatures. This model is widely used in geochemistry, particularly the most recent version, known as the TH (for Tanger and Helgeson, 1988) or revised-HKF model. Considering that a solution is a physicochemical continuum, with $P_{water} = P_{solutes}$, the TH model has been used at negative pressure in order to obtain the thermodynamic properties of aqueous species dissolved in capillary solutions (Mercury et al., 2003). The results obtained for 64 neutral aqueous species, 110 anions and 142 cations show that the partial molar volumes can vary considerably among species, when the P_w decreases. This implies that capillarity

should modify the aqueous complexation equilibria as well as the solubilities of minerals and gases in a species-dependent manner.

2.4. Thermodynamic Properties of Mineral Phases

As for liquid water and aqueous species, the thermodynamic properties of mineral phases can be calculated in capillary conditions by using the mechanical energy term *VdP*. However, the question is open as to the significance of capillary pressure for solids. From a conceptual point of view, four situations must be clearly distinguished.

1. An existing mineral phase is brought into contact with the capillary water, under its own internal pressure. The simplest working hypothesis is that the mineral phase may be at the atmospheric pressure (location near the ground surface), or at the lithostatic pressure (if buried), with the corresponding thermodynamic properties. Meanwhile, the solution is in a capillary state. Thus, one minimizes the thermodynamic potential of the system in an "anisobaric" context between the capillary solution and the mineral phase.
2. A mineral phase can precipitate in a capillary solution when the chemical composition of the solution becomes thermodynamically saturated. If this precipitation takes place on an existing surface (epitaxial-type mechanism), one expects the neoformed phase to be constrained more by the structural characteristics of the solid template than by the surrounding capillary solution. In other words, the epitaxial type precipitation is assumed to take place in an "anisobaric" context.
3. If the precipitation takes place within the capillary solution, and in the case of Wulff's crystal type, the solid/solution system reaches equilibrium by minimizing the shape of the crystal and the pressure difference between precipitating solid and capillary solution: the isobaric context should result in flat/elongated minerals, the anisobaric conditions in curved-type ones (granular. . .).
4. When an equilibrium involves two mineral phases, each one may follow its own behavior. For instance, the mineral initially present in the system is subjected to the atmospheric pressure whereas the neoformed mineral precipitates in isobaric conditions with the capillary aqueous solution. This situation constitutes what is termed hereafter the "dual" context, for which several scenarios can be envisioned.

By way of comparison, Zilberbrand (1997, 1999) has calculated the equilibrium constants of some dissolution/precipitation reactions as a function of the capillary pressure assumed to be constant throughout the whole reaction system, including solids. The trends obtained indicate a reduction in the solubility of the mineral phases (sulfates, carbonates and chlorides) as the capillary pressure decreases. In other words, the concentrations at equilibrium decrease in the small pores. However, this is equivalent to assuming implicitly that the isobaric scenario is the rule, i.e., either dissolving or precipitating solids are at the same pressure as the liquid water.

2.5. Thermodynamic Properties of Gases

The chemical composition of the soil pore atmosphere is not affected by capillary phenomena, except for the decrease in water vapor content. The capillary water is therefore in contact with an atmosphere of (virtually) constant composition. Furthermore, it should be noted that gases are never subjected to the same pressure as the capillary water. This means that, in the UZ, the interaction of gases with capillary solutions is necessarily "anisobaric."

2.6. Geochemical Equilibria

2.6.1. Activity Model Corrections and Debye-Hückel Parameters

In aqueous solutions, dissolved species are not in their standard state and this deviation is assumed by activity model corrections. With respect to relatively dilute solutions, the most widely used ionic activity model corrections are those based on the theory developed by Debye and Hückel (1923). For example, an extended Debye-Hückel model such as the B-dot model (Helgeson, 1969) calculates the activity coefficient γ_i of the aqueous species i as a function of the ionic strength I as follows:

$$\log\gamma_i = -\frac{A_\gamma z_i^2\sqrt{I}}{1+\mathring{a}_i B_\gamma\sqrt{I}} + \mathbf{B}I\,, \tag{6}$$

where

$$I = \frac{1}{2}\sum_i m_i z_i^2; \tag{7}$$

z_i is the charge of the dissolved ion i, $\mathring{a}_i$ is its hard core diameter, $\dot{B}$ is an empiric parameter, and A_γ and B_γ are the Debye-Hückel parameters.

The Debye-Hückel parameters A_γ and B_γ depend on the temperature, the density and the dielectric constant of water according to the expressions given below (Helgeson and Kirkham, 1974). Thus, the speciation calculations in aqueous phase can also be performed in the capillary solutions, where capillary pressure not only affects the equilibrium constants for the reactions but also activity coefficients of aqueous species, independently of the effects due to the salinity (Lassin et al., 2004).

$$A_\gamma = \frac{\sqrt{2\pi N_a\rho}}{\ln(10)\sqrt{1000}}\left(\frac{e^2}{4\pi\varepsilon_0\varepsilon kT}\right), \tag{8}$$

$$B_\gamma = \sqrt{\frac{2e^2N_a\rho}{1000\varepsilon_0\varepsilon kT}}, \tag{9}$$

where ρ ($g\cdot m^{-3}$) is the density of the pure water, which depends on temperature and pressure; $\varepsilon_0 = 8.854\times10^{-12}$ $F\cdot m^{-1}$ is the dielectric permittivity of vacuum; ε (dimensionless) is the dielectric constant (or relative permittivity) of water, which depends on temperature and pressure; $e = 1.602\times10^{-19}$ C is the charge of electron; and $k = 1.381\times10^{-23}$ $J\cdot K^{-1}$ is the Boltzmann constant. A_γ and B_γ have the units $kg^{1/2}\cdot mol^{-1/2}$ and $kg^{1/2}\cdot mol^{-1/2}\cdot m^{-1}$, respectively. The values taken by these parameters at different temperatures and pressures are shown in Table 1.

According to the activity models (e.g., Eqn. 6), other specific parameters may depend on the temperature. This is the case, for

Table 1. Values of the A_γ and B_γ Debye-Hückel parameters at different temperatures and pressures, respectively calculated using equations (8) and (9), and the formalisms of Wagner and Pruss (2002) and Fernández et al. (1997).

	T (°C)/P (MPa)	−150	−100	−50	0.1	50	100	150
A_γ ($kg^{1/2} \cdot mol^{-1/2}$)	−25			0.4846	0.4712	0.4611	0.4519	0.4433
	0		0.5155	0.5022	0.4904	0.4796	0.4696	0.4602
	25	0.5576	0.5383	0.5230	0.5098	0.4980	0.4872	0.4773
	60	0.6090	0.5823	0.5621	0.5453	0.5310	0.5183	0.5068
B_γ ($\times 10^{-10}$) ($kg^{1/2} \cdot mol^{-1/2} \cdot m^{-1}$)	−25			0.3168	0.3191	0.3202	0.3207	0.3209
	0		0.3234	0.3241	0.3245	0.3247	0.3246	0.3244
	25	0.3286	0.3286	0.3286	0.3284	0.3282	0.3279	0.3275
	60	0.3367	0.3358	0.3350	0.3343	0.3337	0.3330	0.3324

example, with the empiric deviation function $\dot{B}$ associated with the B-dot model developed by Helgeson (1969).

By way of illustration, the activity coefficients $\gamma_{\pm z}$ for the ions K^+, Cl^-($\mathring{a}$ = 3 Å, $z = \pm 1$), Na^+ ($\mathring{a}$ = 4 Å, $z = +1$), H^+ ($\mathring{a}$ = 9 Å, $z = +1$), Ca^{2+} ($\mathring{a}$ = 6 Å, $z = +2$) and SO_4^{2-}($\mathring{a}$ = 4 Å, $z = -2$) have been calculated using the B-dot model (Eqn. 6), at 25°C, and data in Table 1 as a function of the ionic strength I (0.001 to 1 eq · kgw^{-1}) and at various pressures (−150 to 150 MPa). The results (Fig. 3) show that the effect of the pressure on the activity coefficients may be significant for ionic strengths greater than or around 0.1 eq · kgw^{-1}. This ionic strength (corresponding to 5.8 g/L of NaCl, for example) can be attained in soil pore water (e.g., Gooddy et al., 2002), especially in the soils sensitive to salinization (Hernandez et al., 1999).

After Figure 3, it should also be noted that according to the Debye-Hückel model, the effect of the ionic strength also depends on the charge z and the distance of closest approach $\mathring{a}$ of the considered ion; it is stronger for high ionic charges and for small minimum approach distances.

For neutral aqueous species, different approaches take into account the effects of ionic strength and temperature on the activity coefficients. These methods are often associated with a given activity model for charged species.

The activity model best suited to concentrated aqueous solutions (high ionic strengths, saying greater than 1 eq · kgw^{-1}) is the Pitzer model (Pitzer, 1973, 1995). This model also includes parameters that depend on the temperature and the pressure which will have to be corrected prior to their use in the capillary domain.

2.6.2. *Fugacity and Solubility of Gases*

Strictly speaking, any deviation in the behavior of gases compared to the ideal situation must consider the fugacity f of the gases instead of their partial pressure p_{gas}. However, the main reactive atmospheric gases considered here, O_2, CO_2, and vapor H_2O at a total pressure of 0.1 MPa, have fugacity coefficients very close to 1 (Appendix). Consequently, in this work, we consider partial pressure and not fugacity.

Gas-aqueous solution equilibria in the UZ are necessarily produced in an anisobaric context since gas pressures vary little, if at all, and in any case cannot be negative (density and pressure of gases are proportional: nil pressure is termed vacuum, i.e., no matter). As an example, partial pressures of the gases O_2, CO_2 and H_2O, at equilibrium with the chemical composition of a river water (Michard, 1989), were calculated as a function of the internal pressure of capillary water. The variations compared to a free solution are positive and clearly species-dependent (Fig. 4). They illustrate that the solubility of the gases increases when the relative humidity (and therefore the water pressure) decreases. Such increasing solubility should promote carbonation and oxidation processes of pore water systems in the UZ.

Mercury et al. (2004) calculated the increasing species-dependent solubility of noble gases (He, Ar, Ne, Kr, Xe) as a function of the internal pressure of the capillary solution. Results show that, under suitable climatic conditions and for finely porous media, the UZ can represent a sink for the atmospheric gases, which is more efficient than saturated aquifers. Accordingly, the authors proposed that the use of rare gases as paleothermometers may require a correction term taking into account their "capillary solubility."

2.7. The "Thermo-zns" Computer Code

A computer code called "Thermo-zns" has been developed (Lassin et al., 2003) to calculate the relevant thermodynamic properties of water, aqueous species, minerals and gases in capillary systems. It is based on two existing computer codes: "Supcrt92" (Johnson et al., 1992) and "Eqtest" (Span and Wagner, 2000). "Supcrt92" calculates standard thermodynamic properties in the SZ and supercritical domains. "Eqtest" calculates thermodynamic properties of water in the SZ and supercritical domains, using the most recent equation of state of water of Wagner and Pruss (2002). In "Thermo-zns" the domain of application is extended to the metastability field of capillary water according to the flowchart shown in Figure 5. New possible input data (compared to Supcrt92) are *RH,* and the choice of mineralogical context by way of the mineral pressure.

3. APPLICATION TO "SIMPLE" EXPERIMENTS

3.1. Boehmite-Bayerite Equilibrium

Verdes and Gout (1987) measured experimentally the temperature-humidity conditions (*T,RH*) of the thermodynamic equilibrium between boehmite and bayerite.

The hydration reaction of boehmite (AlOOH) into bayerite ($Al(OH)_3$) may be written:

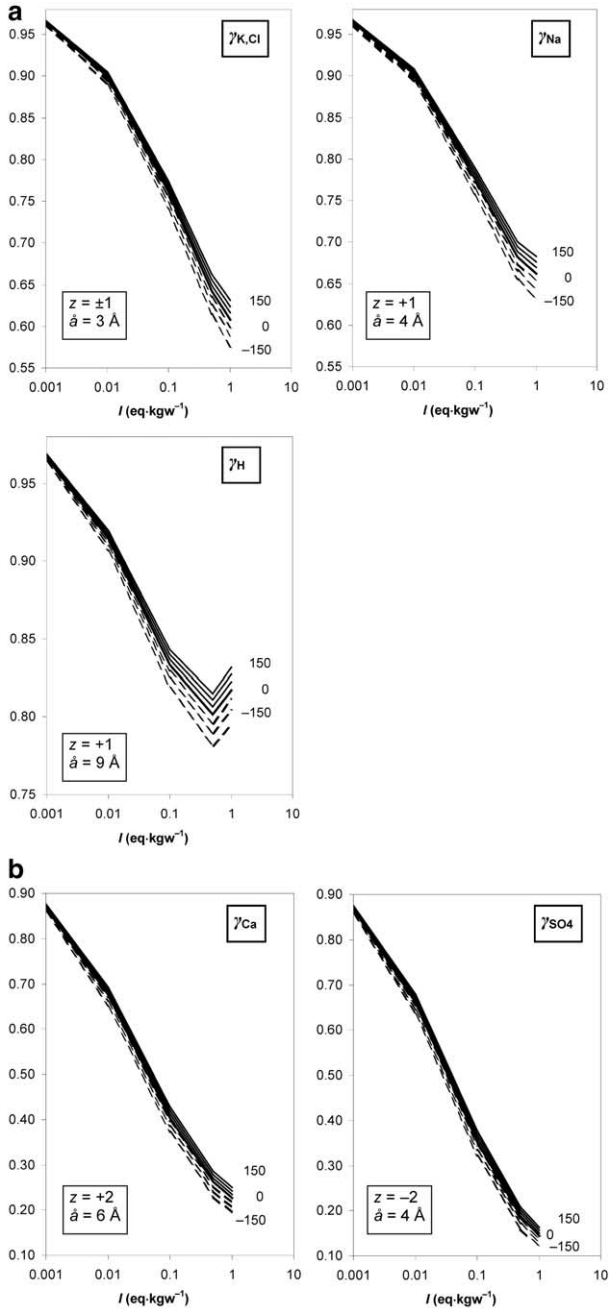

Fig. 3. (a) Activity coefficients γ_i of K^+, Cl^-, Na^+ and H^+, at 25°C, as a function of ionic strength and at different pressures (−150, −100, −50, 0.1, 50, 100, and 150 MPa) according to the B-dot model (Eqn. 6). (b) Activity coefficients γ_i of Ca^{2+} and SO_4^{2-}, at 25°C, as a function of ionic strength and at different pressures (−150, −100, −50, 0.1, 50, 100, and 150 MPa) according to the B-dot model (Eqn. 6).

$$AlOOH + H_2O \Leftrightarrow Al(OH)_3. \quad (10)$$

As shown in Figure 6, the equilibrium temperature between boehmite and bayerite decreases with the relative humidity. With no background electrolyte and at near-neutral pH values, reaction 10 takes place in very dilute solutions ([Al] $\sim 10^{-8}$

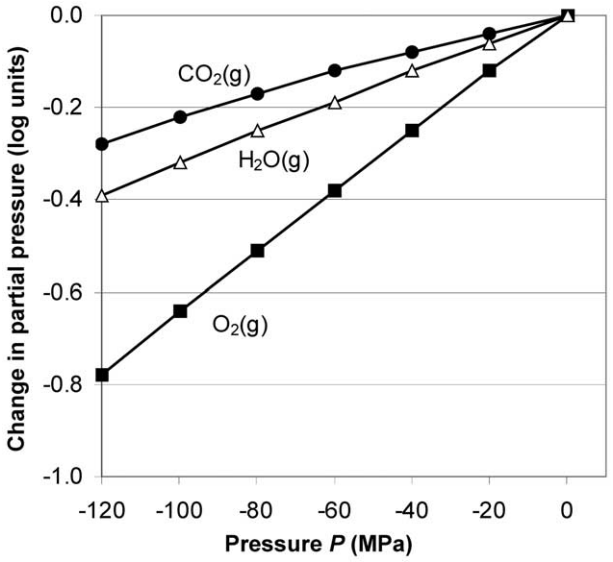

Fig. 4. Variation of the solubility of gases (O_2, CO_2, H_2O) in pore water as a function of the internal pressure of capillary water, at P_{atm} (0.1 MPa) and 25°C. This variation is expressed in terms of variation of partial pressure at equilibrium with constant quantities of dissolved gases.

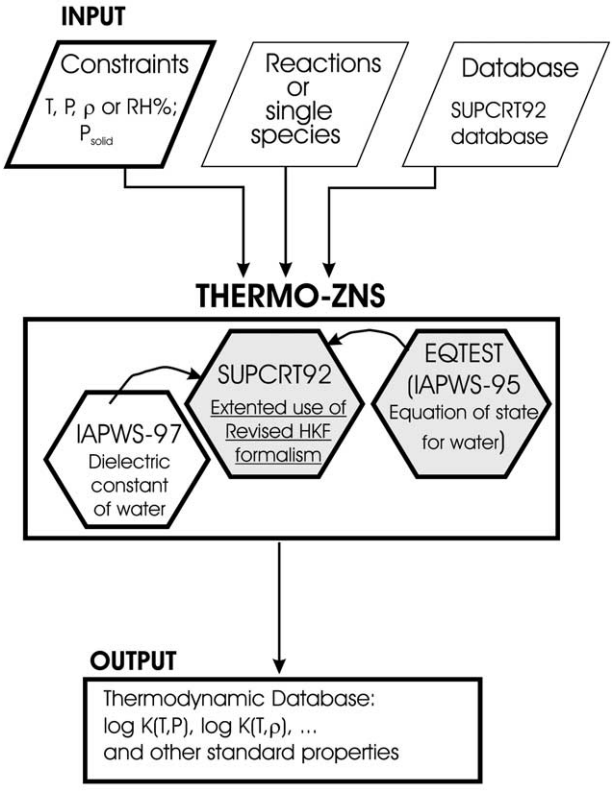

Fig. 5. Synopsis of the overall structure of the "Thermo-zns" computer code. Grey zones represent the core of existing computer codes used to construct "Thermo-zns," i.e., "Supcrt92" and "Eqtest" (see text). Bold lines indicate units modified from these computer codes.

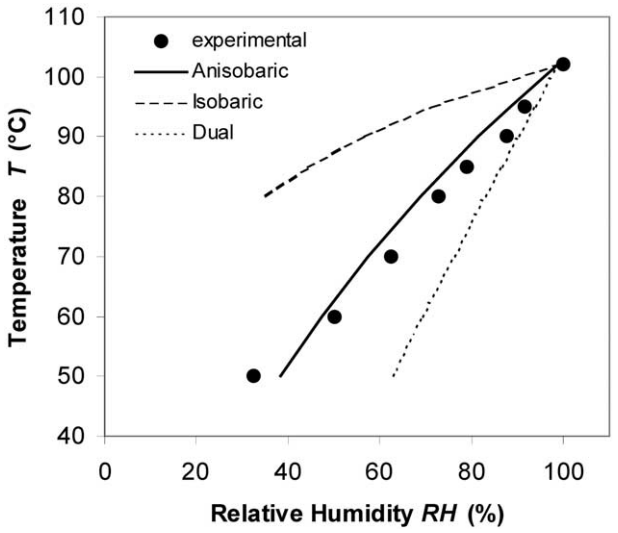

Fig. 6. Equilibrium conditions for the boehmite-bayerite reaction as a function of temperature and relative humidity; the full circles represent the experimental plots according to Verdes and Gout (1987); the curves represent the results of the calculations made in this study according to the isobaric, anisobaric and dual contexts (see text).

mol · kgw^{-1}, ionic strength ~ 10^{-7} eq · kgw^{-1}), i.e., close to standard conditions with $a_w = 1$.

Using the Thermo-zns code, the relative humidity (or the capillary water pressure; cf. section 2) corresponding to the equilibrium of this reaction was calculated for temperatures between 50 and 102°C. The standard thermodynamic properties of the mineral phases under the reference conditions (T_r = 25°C, P_r = 0.1 MPa) are given in Table 2.

Isobaric, anisobaric and dual conditions (see section 2.4) are considered, with the mineral phases subjected to: i) the pressure of the aqueous solution (isobaric context), ii) the atmospheric pressure, different from the pressure of the capillary water (anisobaric context) or iii) the atmospheric pressure for the mineral initially present and the capillary pressure for the neoformed mineral (dual context).

The results obtained from Thermo-zns are compared in Figure 6 with the experimental measurements. It is clear that the anisobaric context accounts very well for the observations down to very low *RH* (24% at 50°C). On the other hand, the trends obtained for the two other contexts deviate from the measured data when relative humidity decreases. This can be explained as follows.

Table 2. Standard thermodynamic properties of boehmite and bayerite, under the reference conditions (T_r = 25°C, P_r = 0.1 MPa), used by Verdes and Gout (1987) and repeated in this work.

Mineral phase	ΔG_f^o [a] (J/mole)	S_f^o [a] (J/mole K)	V^o cm^3/mole
Boehmite	−917100	48.45	19.5[b]
Bayerite	−1158100	68	31.2[c]

[a] According to Verdes and Gout (1987).
[b] According to slop98.dat (Shock et al., 1997).
[c] Deduced from the density, equal to 2.5 g/cm^3, according to the webmineral.com website (http://webmineral.com/).

Boehmite is initially present in the system so that (section 2.4) it should remain subjected to its initial pressure, which is the atmospheric pressure. The anisobaric context should be expected and actually is the most suitable to account for this experiment. As a matter of fact, an isobaric hypothetical scenario results in a greater solubility of the boehmite than that indicated by the experiment (Fig. 6). On the other hand, the dual context tends to favor the bayerite to a greater extent than that shown by the experimental results. This may suggest that during this experiment, bayerite is formed by epitaxial type growth, either from the boehmite itself, or from other substrates that are non reactive but initially present in the system. This explanation could be checked by a microscope analysis of the solid samples.

3.2. Oxidation of Pyrite in an Atmosphere with Controlled Relative Humidity

Other experiments studied the oxidation of pyrite at different relative humidities lower than 100% (Borek, 1994; Guevremont et al., 1998; Todd et al., 2003; Jerz and Rimstidt, 2004). Such conditions occur in several environmentally important contexts such as those related to acid mine drainage (Blowes et al., 1991; Jambor and Blowes, 1998; Nordstrom and Alpers, 1999). The humidity and temperature conditions imposed by the different authors are summarized in Table 3. This table also gives the results obtained for the calculations of the internal pressure and density of the capillary water, as well as the Kelvin radius r_K (Eqn. 4). This latter parameter, calculated for a nil water/solid contact angle, gives an indication of the maximum size of the pores saturated with water (neglecting the wetting film thickness). The surface tension σ, which depends on the temperature, is calculated in accordance with the recommendations of the IAPWS (1994). Based on Figure 1, the internal pressure of capillary water and the corresponding Kelvin radius are given as a function of the relative humidity (Fig. 7).

Data given in Table 3 and Figure 7 lead to the following conclusions:

1. A small variation in the vapor partial pressure (i.e., *RH*) results in significant variations in water pressure and Kelvin radius. Furthermore, the higher the relative humidity, the greater the variability of the latter parameter.

2. The temperature measurement is very important. Guevremont et al. (1998) did not indicate the laboratory temperature at which their experiments were carried out. Therefore, as one can expect in a laboratory, the temperature is here assumed to lie between 20 and 25°C. This temperature difference is reflected in a relative humidity comprised between 98.3 and 72.6%, respectively, and therefore water pressures range from −2.3 to −43.4 MPa.

As expressed by Eqn. 2, the relative humidity at equilibrium with a capillary solution includes the contributions of both the internal pressure of water and the salinity of the solution (i.e., the activity of water). Here, Eqn. 2 has to be rewritten to define an apparent relative humidity *RH** from which the capillary water pressure may be calculated using the Thermo-zns code (Lassin et al., 2003):

Table 3. Experimental conditions for studying the oxidation of pyrite in a humid atmosphere, according to various authors; internal pressure P, density ρ of the capillary water and corresponding Kelvin r_k radius.

Ref.	T(K)	pH_2O (MPa)	RH (%)	P(MPa)[e]	ρ (g/m^3)[e]	σ (mJ/m^2)	r_k (nm)
—	293.15	$2.34 \cdot 10^{-3}$ [b]	100	$7.14 \cdot 10^{-3}$	998200	72.74	-10^9
[1][a]	293.15	$2.3 \cdot 10^{-3}$	98.3	−2.31	997100	72.74	−61.84
[2]	293.15	$2.0 \cdot 10^{-3}$	85.5	−21.02	988300	72.74	−6.83
—	295.15	$2.65 \cdot 10^{-3}$ [b]	100	$10.17 \cdot 10^{-3}$	997700	72.43	-10^9
[3]	295.15	$2.09 \cdot 10^{-3}$ [c]	79	−31.75	982800	72.43	−4.54
[3]	295.15	$1.86 \cdot 10^{-3}$ [c]	70	−47.86	974800	72.43	−3.03
[3]	295.15	$1.33 \cdot 10^{-3}$ [c]	50	−91.97	951100	72.43	−1.60
[3]	295.15	$9.01 \cdot 10^{-4}$ [c]	34	−141.12	920000	72.43	−1.06
—	298.15	$3.17 \cdot 10^{-3}$ [b]	100	$11.25 \cdot 10^{-3}$	997000	71.97	-10^9
[4]	298.15	$3.07 \cdot 10^{-3}$ [c]	96.7	−4.58	994900	71.97	−31.34
[1][a]	298.15	$2.3 \cdot 10^{-3}$	72.6	−43.41	976500	71.97	−3.35

[1]: Guevremont et al. (1998) — [2]: Todd et al. (2003) — [3]: Borek (1994) — [4]: Jerz and Rimstidt (2004).
[a] Since the laboratory temperature is not specified by the authors, two possibilities have been envisaged, 20 °C and 25 °C.
[b] Saturation vapor pressure ($2.34 \cdot 10^{-3}$ MPa at 20 °C, $2.65 \cdot 10^{-3}$ MPa at 22 °C, $3.17.10^{-3}$ MPa at 25 °C).
[c] Relative humidity set with the aid of a saline solution (ref. [3,4]), and not by a partial pressure of H_2O; the value given is the result of the calculation $pH_2O = p_0 \times RH/100$.
[e] Calculated using the Thermo-zns code.

$$RT \ln \frac{RH^*}{100} = RT\left(\ln \frac{p}{p_0} - \ln a_w\right) = \int_{P_r}^{P} V_w \cdot dP, \qquad (11)$$

However, the ionic strengths encountered hereafter (~0.7 eq $\cdot$ kgw^{-1}, see below), result in a water activity equal to 0.994 and therefore, according to Eqn. 11, RH^* values deviate from the relative humidities, RH, given in Table 3 by 0.6%. The appearance of the correspondence curve between the relative humidity and the capillary pressure in Figure 7 suggests that such small relative humidity deviations do not have an effect on the water pressure despite the fact that the Kelvin radius at high RH can be affected. Focusing here on geochemical calculations rather than on pore geometry, it was decided not to take account of this "apparent" relative humidity effect in the remainder of this work. However, in solutions of higher salinity, this correction must be taken into account (Benavente et al., 2004).

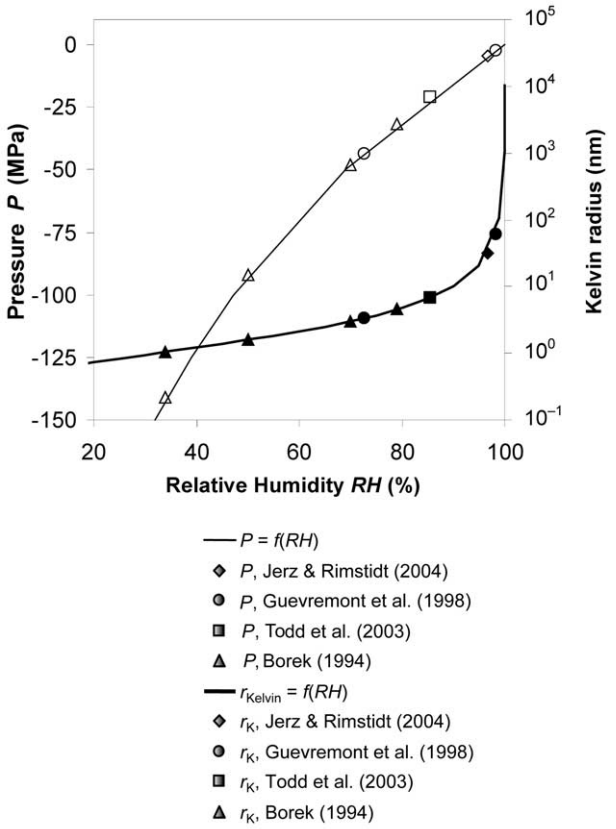

Fig. 7. Internal pressure of capillary water (P) and Kelvin radius (r_K) corresponding to the experimental conditions of the cited studies.

Data given in Table 3 allow the calculation of the thermodynamic properties of the aqueous species, gases and mineral phases that may be involved in the pyrite oxidation process, as well as the relevant Debye-Hückel parameter A_γ. The various authors cited above have observed that in atmospheres of varied humidity, the pyrite oxidation at the mineral surfaces results in the replacement by iron sulfate. The reactions that need to be taken into account are therefore:

$$FeS_2 + H_2O + 3.5\ O_{2,g} \Leftrightarrow Fe^{2+} + 2\ SO_4^{2-} + 2\ H^+ \qquad (12)$$

$$FeSO_4 \Leftrightarrow Fe^{2+} + SO_4^{2-} \qquad (13)$$

$$FeS_2 + H_2O + 3.5\ O_{2,g} \Leftrightarrow FeSO_4 + SO_4^{2-} + 2\ H^+ \qquad (14)$$

and

$$O_{2,g} \Leftrightarrow O_{2,aq} \qquad (15)$$

The equilibrium constants for reactions 12 to 15 are calculated from Table 3, as a function of the isobaric and anisobaric conditions. For reaction 14, which involves two mineral phases, the dual context is also tested. The standard thermodynamic data are from Shock et al. (1997), integrated in the slop98.dat database developed by the GEOPIG team for the Supcrt92 (Johnson et al., 1992) calculation code, and thus adapted to the Thermo-zns code. Only the properties of the iron sulfate, absent from slop98.dat, were taken from the Wagman et al. (1982) database. The thermodynamic properties of all of the aqueous species of the chemical system Fe-S-H_2O contained in the slop98.dat database, i.e., nearly 40 aqueous species, have also

been calculated under the temperature and pressure working conditions (Table 3).

Output data from Thermo-zns are integrated into the Phreeqc-type database (Parkhurst and Appelo, 1999) in order to carry out speciation and saturation index calculations that simultaneously take into account the effects of capillarity and salinity. In fact, the imposed conditions are the partial pressure of atmospheric oxygen: $pO_2 = 0.021$ MPa, and a limited quantity of pyrite subjected to the oxidation in such a way that the ionic strength of the final solution (~0.7 eq/kgw) remains within the domain of validity of the Davies activity model, integrated by default in the Phreeqc code. In contrast, the iron sulfate precipitation conditions correspond to very high ionic strengths and as such the Davies model (Davies, 1962) is no longer valid. Actually, the relevant formalism is the Pitzer one which has still to be adapted to the UZ as indicated in section 2.6.1. Under the conditions considered above, the calculated pH is very acid (1.8 ± 0.2) and the redox potential (*pe*) is very high (19.4 ± 0.1) indicating oxidizing conditions.

Calculating the ionic activity product, *Q,* and the equilibrium constant, *K,* for reaction 14 at the various relative humidities (*RH*) and temperatures (*T*) leads to the *Q*/*K*(*T*,*RH*) ratio, which measures the deviation of the reaction from thermodynamic equilibrium. The variation in this *Q*/*K* ratio as a function of the relative humidity provides an indication of the change in the "driving force" of the reaction. This variation, δ (log *Q*/*K*), is defined by:

$$\delta(\log Q/K) = \log Q/K(T, RH) - \log Q/K(T, 100\%). \quad (16)$$

In the same way, the variation in the equilibrium constant for the reaction 14 as a function of the relative humidity may be defined by:

$$\delta(-\log K) = \log K(T, 100\%) - \log K(T, RH). \quad (17)$$

In reaction 14, suggested by Borek (1994), one can expect the following configurations. The pyrite initially present is assumed to be subjected to atmospheric pressure. As for the iron sulfate, Jerz and Rimstidt (2004) pointed out that its precipitation was accompanied by the passivation of the pyrite surface. That leads to expect that the iron sulfate precipitates at the very surface, which corresponds after section 2.4 to an epitaxial anisobaric context. To illustrate the flexibility of the model, it is proposed a supplementary refinement by assuming that the iron sulfate does not undergo the structural constraints of its substrate but precipitates under isobaric conditions. The variations in the equilibrium constant for the reaction 14 and the *Q*/*K* ratio as a function of the relative humidity, in the three contexts considered, are shown in Figure 7. It should be noted that in real situations, this question of scenario must be chosen according to the indications of microscopic studies of the mineralogical assembly.

The lowest *RH* tested by Borek (1994) correspond to an arid climate (cf. NOAA climatic data for Las Vegas, Texas, or Phoenix, Arizona, for example, available at http://www.ncdc.noaa.gov/oa/ncdc.html). The highest *RH* correspond to cool to temperate humid climates (cf. NOAA climatic data for Quillayute in Washington State, where $65 < RH < 95\%$, and $2 < T < 14$°C, for year 2003, for example) and humid tropical climates (cf. NOAA climatic data for Pohnpei in the Caroline Islands, where $75 < RH < 95\%$, and $T \approx 27$°C, for year 2003, for example). These *RH* are plotted in Figure 2 to give an idea of the corresponding extent of water metastability (proximity of the spinodal curve).

Figure 8 shows that the variation δ(log *Q*/*K*) is negative at every *RH,* whatever the temperature (20–25°C) and the chosen context (isobaric, anisobaric or dual). The iron sulfate ($FeSO_4$) is always favored over the pyrite (FeS_2) in capillary conditions and at constant O_2 partial pressure. This stabilization increases as the relative humidity decreases and its magnitude depends on the chosen context. The least favorable context is the anisobaric one, in which the δ(log *Q*/*K*) is equal to −0.1, −0.2 and −0.8, under the respective conditions of (20°C, 85.5%), (25°C, 72.6%) and (22°C, 34%). The most favorable context is the dual context in which the δ(log *Q*/*K*) is equal to −0.25, −0.5 and −1.8, under the same conditions as previously. These values are significant and, for the lowest relative humidities or the contexts that are the most favorable to the stabilization of the solid iron sulfate ($FeSO_4$), they are of the same order or greater than the uncertainties that exist between various data sources such as Naumov et al. (1974), Helgeson et al. (1978), Shock and Helgeson (1988) and Shock et al. (1989, 1997) for slop98.dat, Wagman et al. (1982), Robie and Hemingway (1995), and Chivot (2004). In fact, the mean equilibrium constant corresponding to the reaction 14, calculated from the different sets of data, is log K = 204.5 ± 0.6 (under the reference conditions). If one limits oneself only to the sources that provide all of the required data (Naumov et al., 1974; Robie and Hemingway, 1995), the average value of the equilibrium constant becomes log K = 203.7 ± 0.4.

Comparing the variations in the ratio δ(log *Q*/*K*) to the variations δ(−log *K*) (Fig. 8) highlights the stabilizing role of the speciation of the capillary solution on the system (solid iron sulfate + SO_4^{2-} + H^+) relative to the system (pyrite + $O_{2,g}$ + H_2O). The combined effect of the speciation and the equilibrium constant is amplified when both effects go in the stabilizing direction, that is with the isobaric and dual contexts. In the anisobaric context, the effect of the speciation reverses the trend observed for the variation of the equilibrium constant, which would suggest a slight stabilization of the system (pyrite + $O_{2,g}$ + H_2O) compared to the system (solid iron sulfate + SO_4^{2-} + H^+) when the relative humidity decreases. Distinct contributions can be described more precisely.

3.2.1. The Relative Stabilization of Pyrite and Iron Sulfate

Isobaric "tensile" minerals are stabilized in capillary solutions. In the dual context, only the iron sulfate is subjected to the capillary pressure whereas the pyrite is not, favoring the respective stability of the former over the latter. Consequently, the trend to stabilization (i.e., the reduction in solubility) of the iron sulfate obtained for the isobaric context is amplified in the dual context.

3.2.2. The Evolution of the Solubility Product of O_2

This evolution (Reaction 15 and Section 2.6.2) corresponds to an increasing solubility of the gaseous oxygen when the relative humidity decreases. This effect must be added to the higher diffusion of gaseous oxygen in air, which is ten thousand times greater than the diffusion of aqueous oxygen in water

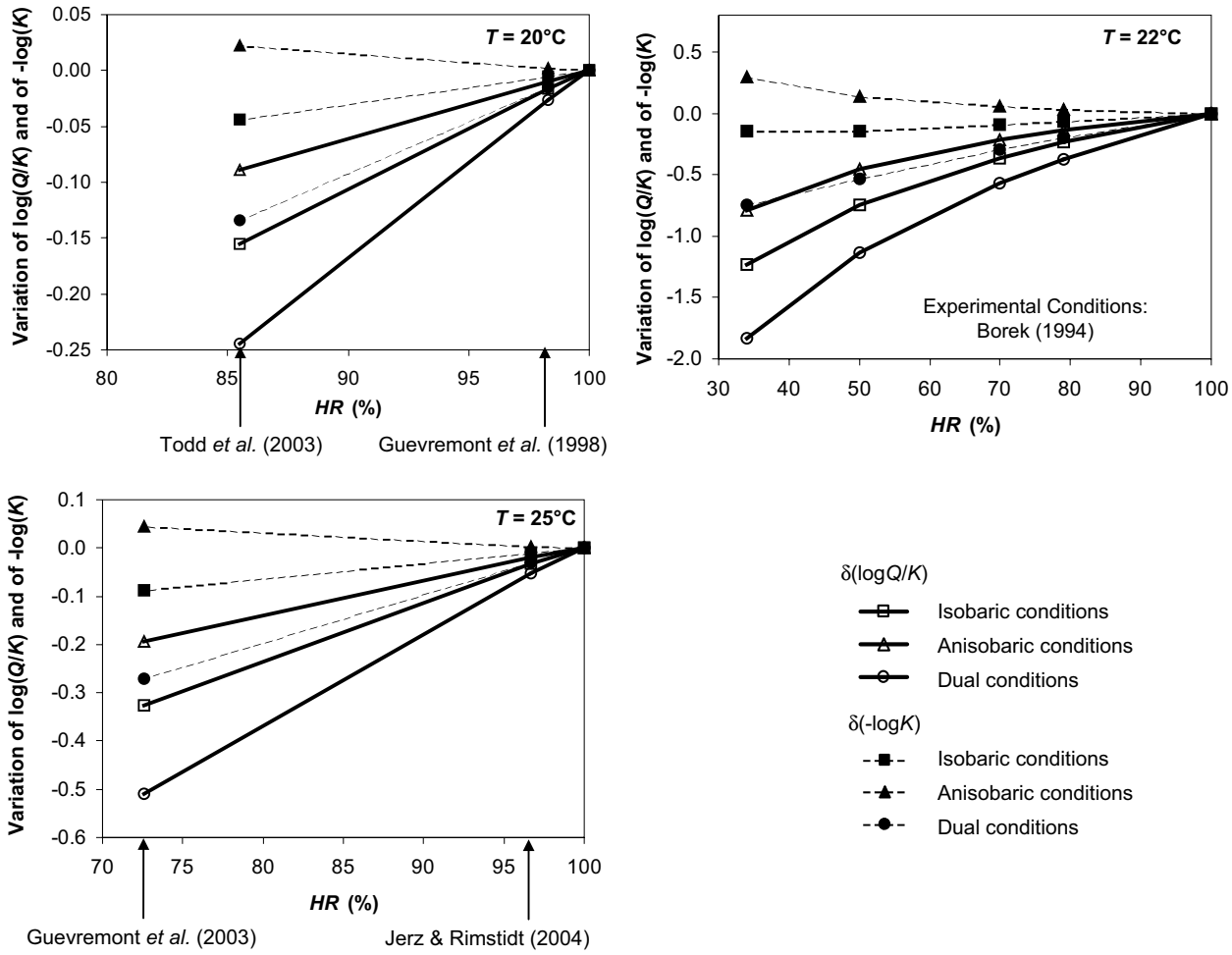

Fig. 8. Variation in the log Q/K ratio for reaction 14 as a function of relative humidity, at 20, 22 and 25°C, for an ionic strength close to 0.7 eq · kgw^{-1}, according to the isobaric, anisobaric and dual contexts described in the text. For comparison, the variation in the equilibrium constant for reaction 14 is also shown as a function of relative humidity at various temperatures and for the different contexts.

(Hecht and Kölling, 2002), both effect favoring the oxygen supply for the geochemical systems in the UZ.

The greater solubility of oxygen agrees with the observations made by Jerz and Rimstidt (2004) who showed that the initial consumption rate of oxygen is higher at 96.7% *RH* than the conventional rate of an aqueous phase oxidation reaction (*RH* = 100%). However, given the low amount of water present in the system, the capillary solution rapidly reaches saturation with respect to the iron sulfate. As a matter of fact, Jerz and Rimstidt (2004) reported a severe restriction of further oxidation by as much as 1 or 2 orders of magnitude (surface passivation). These observations corroborate those of Borek (1994), who noted a maximum amount of altered pyrite at about 70% humidity. At higher relative humidities, the capillary effects are less intense and, consequently, only amplify the oxidation to a small extent compared to the SZ. Conversely, at lower relative humidities, the quantities of water in the porosity are low and the capillary effects are strong. The iron sulfate ($FeSO_4$) reaches saturation rapidly and causes passivation of the pyrite surface. Hollings et al. (2001) obtained experimental results that also highlight a maximum rate of oxygen consumption by the pyrite for a given range of relative humidities. However, these authors plotted this maximum between 12 and 25% *RH* at 20°C. This discrepancy with the results of Borek (1994) is probably related to the experimental conditions. The former experiments (Hollings et al., 2001) were carried out on a particle size fraction between 0.1 and 0.6 mm. The sample was previously dried at 105 °C before rehydration. The latter experiments (Borek, 1994) were performed on pure natural pyrites, ground into smaller particle sizes (between 63 and 75 μm) and washed with hydrochloric acid.

The interpretations must thus be related to the experimental conditions. For instance, when there is an outflow of the solution from the porosity, a leaching mechanism can maintain a steady state far from equilibrium, preventing the surface pyrite from passivating. Indeed, Hecht and Kölling (2002) performed the complete leaching of the pyrite contained in an unsaturated column of soil consisting of silty sand for a period of around 200 days. Furthermore, Fennemore et al. (1998) and Hollings et al. (2001) have demonstrated experimentally that the size of the grains, and therefore the specific surface of pyrite, is also a parameter that affects the reactivity of the mineral to oxidation.

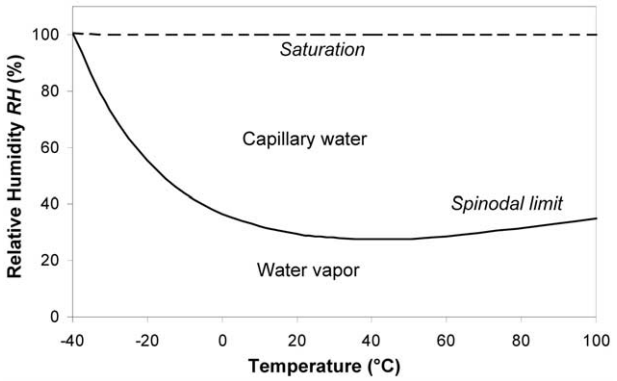

Fig. 9. Metastability domain of capillary water as a function of temperature and relative humidity of the air.

These results illustrate the potential contribution of the thermodynamic approach of the aqueous capillary solutions to the understanding of the geochemistry of the UZ. The effects of capillary pressure and chemical composition of the solution are clearly identified in this approach. In particular, activity coefficients are constrained in a rigorous manner. The role of the gases is emphasized, as well as the "crystalline strategy" of the mineral phases (precipitation within the solution, epitaxial type growth, for example).

4. DISCUSSION

4.1. Limitations in the Range of Applications

The lowest calculated spinodal pressure is equal to −179.4 MPa at 57°C according to the equation of state of Wagner and Pruss (2002). It is very close to that measured at 42°C in a fluid inclusion (−180 MPa) by Zheng et al. (1991) which is, at the moment, the lowest measured pressure. A correspondence illustrating the theoretical limit of the existence of the capillary water sensu stricto can be established with the relative humidity of the air (Fig. 9). It thus appears that a system at equilibrium with an atmosphere of relative humidity less than 30%, around 25°C, would no longer contain pure capillary water. This does not exclude the possibility that water adsorbed at the surface of the solids may subsist (Mercury and Tardy, 2004).

The latter authors pointed out that the present state of development of the proposed approach is limited to the capillary water sensu stricto, in other words not including film water. Consequently, the extension of the application of the revised-HKF model for calculating the thermodynamic properties of the aqueous species only concerns the capillary solutions, not the adsorption films. However, from a theoretical point of view, it should be noted that adsorption films adjust their thickness such that the chemical potential equals that of the water vapor (disjoining pressure concept; see for example Derjaguin et al., 1987). This is analogous to the adjustment of radii by capillary meniscus. In this case, film water (with given thickness), capillary water (with given radius) and water vapor (with given *RH*) have the same Gibbs free energy along the (*P,T*) plots of equilibrium. However, the forces underlining the tensile state of these metastable waters are different. Capillary water obeys the liquid-liquid cohesion and thus obeys the equation of state in its whole domain of existence. Film water undergoes additional contributions from the adjoining solids (surface forces) and, if its chemical potential equals that of the equilibrium water vapor, the other physicochemical properties cannot be predicted according to the equation of state. It should also be noted that, given Eqn. 2, one may expect that some relatively concentrated capillary solutions may be in equilibrium with lower relative humidities than those corresponding to the spinodal. Indeed, this equation means that, for a capillary aqueous solution at equilibrium with a constant relative humidity, a decrease in the water activity due to the salinity of the solution allows the intensity of the capillary pressure to be reduced. For instance, the calculated spinodal for a 1 molal NaCl solution is actually lower than that of pure water (Green et al., 1990). Notwithstanding this, in the present state of development of the approach, it is preferable to consider systems that do not reach the liquid water-vapor spinodal limit.

4.2. Behavior of Capillary Water

The density of the capillary water decreases with pressure at constant temperature, according to the equation of state. This actually reflects the stretched state of the capillary water under the humid air-water interface, the concavity of which is directed towards the air. This decreasing density results in a decreasing dielectric constant of the capillary water (after the equation of Fernández et al., 1997). This is in agreement with various experimental studies (Boyarskii, 2002; Seyfried and Murdock, 2004). They show a reduction in the dielectric constant of water with the number of hydration water layers or with the water content of the porous medium and hence, by extension, with the relative humidity. The dielectric constant is a parameter that measures the ability of a solvent to dissolve minerals. A decreasing dielectric constant corresponds to a lowering capacity of the solvent to dissolve solids (Wasserman et al., 1995; Byrne and Laurie, 1999).

4.3. Mineral Solubility in UZ and Limits Imposed by the Anisobaric/Isobaric Hypotheses

The examples reported above show that the isobaric context maximizes the decreasing solubility of the minerals in capillary systems. Conversely, the anisobaric context has a tendency to oppose the reduction in the solubility of the mineral phases. In other words, even if one mineral is not affected by the capillary state of the solution, the chemical capability of the latter is affected which is reflected by the change of the equilibrium constant. Whenever chemical reactions involve several mineral phases, the variation in their relative stability also depends on the manner the mineralogical assembly will be arranged (see section 3).

According to the revised-HKF theory, the simultaneous variation in the dielectric constant and the density of water plays a role in the variation in the Gibbs free energy of aqueous species as a function of the capillary pressure. In other words, the capillary pressure modifies the complexation equilibria between aqueous species. This adds a new factor in the evolution of the solubility of minerals as a function of the capillary pressure.

The capillary pressure of the solution increases the solubility of rare and reactive gases, at odds with the general trend obtained for minerals. The dissolution reaction of a gas necessarily takes place

in an anisobaric context. The increase in its solubility is therefore associated with the stabilization of the aqueous species involved in the dissolution reaction. Indeed, this behavior results from the lowering of the Gibbs free energy of $O_{2,aq}$, $CO_{2,aq}$ and H_2O when the capillary tension increases, due to the positive molar volume of these aqueous species and solvent. The aqueous species for which the molar volume is negative show the opposite behavior. As an example, the ion Ca^{2+} has a molar volume $V°$ of -18.2 $cm^3 \cdot mol^{-1}$ and a standard Gibbs free energy of formation from elements, ΔG_f°, of -552.8 kJ·mol^{-1} at 25°C, 0.1 MPa. At 25°C, -100 MPa, $V°$ and ΔG_f° are respectively equal to -30.1 $cm^3 \cdot mol^{-1}$ and -550.5 kJ $\cdot$ mol^{-1}. This increase in the ΔG_f° of Ca^{2+} with the reduction in the pressure results in a destabilization of the aqueous ion in a drying context. Under the same conditions, the molar volume of aqueous oxygen and its standard Gibbs free energy of formation from elements go respectively from 30.4 to 32.8 $cm^3 \cdot mol^{-1}$ and from 16.6 to 13.4 kJ $\cdot$ mol^{-1}. This reduction in the ΔG_f° of $O_{2,aq}$ with the decrease in the pressure results in a stabilization of the aqueous ion in a dry atmosphere context.

When the ionic strength of the solution increases, the oxygen becomes less soluble (salting out effect). The concentration of dissolved oxygen in a very dilute solution in equilibrium with the atmosphere ($pO_2 = 0.02$ MPa) is 2.53×10^{-4} mol $\cdot$ kgw^{-1}. In concentrated NaCl solutions, the activity coefficient of aqueous O_2 can be calculated after Clegg and Whitfield (1991). For instance, in a 1 molal NaCl solution, the calculated concentration of dissolved oxygen in equilibrium with atmospheric gases is only 1.86×10^{-4} mol $\cdot$ kgw^{-1}. This difference in concentration corresponds to a difference in the energy of the oxygen dissolution between the dilute and the concentrated solutions. This energy difference is expressed by the activity coefficient of the aqueous oxygen, which is 0.3 logarithm unit in the concentrated solution (and 0 in the dilute one). The capillary effect on the thermodynamic equilibrium constant is just the opposite, favoring the solubility. Indeed, a calculation using Thermo-zns indicates that the same energy difference (with the opposite sign) as that produced by the above salinity is obtained for a relative humidity close to 70% (i.e., a capillary pressure of around -50 MPa). The opposing effects of the 1 molal NaCl salinity and the 70% *RH* capillarity neutralize each other so that the solubility of the oxygen remains constant. Depending on their relative importance, they can therefore give rise to a variety of situations and thus illustrate the diversity/flexibility offered by this model for interpreting real cases. This should also allow a better evaluation of the quantity of dissolved oxygen, which is often underestimated due to its presumed low solubility (Hecht and Kölling, 2002).

It is important to highlight that the whole reasoning developed above is homogeneous to that developed in the saturated geological systems. This illustrates the continuity of the geochemical processes between the zones saturated and not saturated with water, and the strong interest of using a formalism that respects this continuity. Furthermore, it appears that the definition of the different (an)isobaric contexts opens the way to numerous new ways of interpreting the observed equilibria and of understanding their guiding mechanisms.

4.4. Limits of the Approach Due to Lacking Input Data

One specificity of the chemistry of the UZ is the low value of the hydraulic conductivity correlated of course with the intensity of capillary tension (for why it is often termed as suction). This constitutes an obstacle in experimental terms since tensile water cannot be extracted easily, in a non disrupted manner and with a sufficient volume of samples. To this difficulty may be added local heterogeneities that may give rise, in the same medium, to the coexistence of phases that are exclusive from the sole point of view of thermodynamics.

Nevertheless, indirect techniques have already been used, based on controlled equivalences in temperature and relative humidity (Verdes and Gout, 1987), or on measurements of the consumption of reactive gases (O_2) during pyrite oxidation reactions (Jerz and Rimstidt, 2004). Various methods for observing in situ and interpreting the observations may also provide interesting information. This is true for the work of Mulyanto and Stoops (2003) and Tardy and Novikoff (1988). The latter authors have, for example, described the local mineralogical organization of a lateritic profile. They observed that the kaolinite precipitated filling the small pores (~ 1 μm) and that the gibbsite precipitated filling the larger pores (>10 μm).

Although the model seems interestingly flexible for the surface domain, important experimental developments are now necessary to check the validity of the whole frame and its predictive capability. For example, Benavente et al. (2004) have recently carried out a study on the role of the structure of pores on the crystallization of salts in a porous material not saturated with water. In this study, a specific experimental protocol was developed to take account of capillary and osmotic effects in a distinct manner, as well as observing the mode of precipitation of the different salts (homogeneous nucleation for mirabilite, heterogeneous nucleation for thenardite and halite). The authors concluded by emphasizing the major role of the size of the pores of the materials on the geochemical dynamics of their media. Such kind of studies should, in particular, allow to define more physically the notions of isobaric, anisobaric and dual contexts used in the present study.

The key point of the whole approach is the continuity of physical and chemical mechanisms from the SZ up to the UZ, expressed in a formal manner through Eqn. 2. Actually, in the SZ, in surface or subsurface conditions (free water at or close to the reference pressure P_r, itself very close to the atmospheric pressure), the integral term of the right-member of Eqn. 2 is zero and, therefore, relative humidity may be assimilated to water activity.

When the system becomes non saturated with water (UZ), the internal pressure of the capillary water decreases in such a way that this integral term is no longer zero. Consequently, the water activity can no longer be assimilated to the relative humidity of the air.

It is worth outlining that, when the pressure of the water saturated system increases (submersion potential), the simultaneous use of the water activity (due to the effects of the salinity of aqueous solutions) and the mechanical stress of pressure is both traditionally and widely accepted. This type of system may be monophasic, in the sense where the water vapor is no longer expressed. Nevertheless, the equivalent relative humidity may be evaluated numerically.

5. CONCLUSION AND OUTLOOK

The approach followed through this work was based on the interpretation of capillary effects in terms of the internal pressure

of capillary water. The first objective of the present work was to integrate the osmotic aspects (i.e., linked to the chemical composition of the solutions) to the capillary processes, the second to apply this overall model to laboratory case studies or real systems. Firstly, the formal framework allowing the calculations of geochemical equilibria in the UZ systems was defined, with a clear distinction of the capillary and osmotic effects, in a simultaneous but distinct manner. The calculations required to gain the second applied objective were carried out through the combination of two calculation codes.

The first code, named Thermo-zns calculates the thermodynamic properties of all the compounds of a chemical system at all pressures and temperatures. It was developed on the basis of the Supcrt92 code (Johnson et al., 1992) to extend the calculations of equilibrium constants to the negative pressures of the capillary domain. It is also able to evaluate the variations as a function of the temperature and pressure, of the Debye-Hückel coefficients used in conventional models for calculating the activity coefficients of charged aqueous species. The relative humidity is integrated as an additional parameter. The different configurations related to the mineralogical assemblies and to the crystal strategies of nucleating-deliquescing, dissolving/precipitating, are also provisioned in an open way, focused at the moment on the "solid pressure" parameter.

The second code used is Phreeqc (Parkhurst and Appelo, 1999) in order to carry out speciation and saturation index calculations. The databases used with this code were established, for each pressure considered, from results obtained using Thermo-zns. The original thermodynamic database is that associated with Supcrt92, i.e., "slop98.dat."

The approach was applied to two actual cases based on the results of experimental studies: a study of the hydration of boehmite into bayerite, as a function of temperature and relative humidity; three experimental studies on the oxidation of pyrite in atmospheres with several relative humidities.

The results obtained show that the proposed approach can indeed be applied to real cases and that the capillarity can contribute, at a significant level, to the evolution of the chemical equilibria. They also highlight the possibility and the necessity to distinguish, in a clear manner, the capillary effects from those linked to the salinity of the aqueous solutions. This distinction refines the manner with which the chemical equilibria of mineralogical assemblies may be interpreted. The flexibility introduced owing to the isobaric and anisobaric contexts is also promising and favorably compares to available observations. However, it appears clear that some specific experiments should be planned with the whole set of measurements and observations, to check the capabilities of the model in a nonambiguous manner.

The results gained here also show that the effects linked to the capillarity must be taken into account in an overall manner in order to measure their importance. This means that, in order to interpret the behavior of actual complex systems, not saturated in water, one has to integrate the effects of the capillarity on the speciation in solution and the thermodynamic stability of individual phases, all these effects being linked to the salinity.

It is also clear that the (inorganic) geochemistry of the UZ must take the physical dimension linked to capillary phenomena into account. The continuous passage from positive values to negative values for the water pressure enables to deal with the chemistry of the solutions of the saturated and non saturated zones in a homogeneous manner. Furthermore, this approach is in line with those adopted in other scientific fields such as the physics and chemistry of interfaces and surfaces, colloids, emulsions, etc. However, it appears necessary to complete the capillary approach of the geochemistry of the UZ by explicitly including the role (i) of the adsorption films including electrostatic surface phenomena and (ii) of the reactional interface sensu stricto, in other words the very first layer(s) of water deposited or with a strong interaction with the solid. Although we are here touching on the application limits of macroscopic thermodynamics, one may imagine that the equilibrium constants for the volumetric reaction mixture ("the bulk") must be treated with energies that characterize the interfacial phases.

Finally, the dependence on the chemical composition of a capillary solution to the distance from the walls of the pore could also be taken into account by means of a suitable thermodynamic formalism (Basu and Sharma, 1994; Manciu and Ruckenstein, 2003; Ruckenstein and Manciu, 2003).

Acknowledgments—M. Zilberbrand, A. F. White and D. A. Sverjensky are gratefully acknowledged for their precise and patient reviews, which have considerably improved the writing style and the scientific content of the initial manuscript. The authors are indebted to W. Wagner who kindly provided the software "Basic Package IAPWS-95," containing the "Eqtest" computer code and to D. Guyonnet for his help in improving the English style. A. L. is indebted to Y. Tardy who introduced him to the geochemistry of UZ. Funding was provided by BRGM (French Geological Survey) through the Research Division Project, "MODHYC."

Associate editor: D. A. Sverjensky

REFERENCES

Barrett E. P., Joyner L. G., and Hallenda P. P. (1951) The determination of pore volume and area distributions in porous substances: I. Computations from nitrogen isotherms. *J. Am. Chem. Soc.* **73,** 373–381.

Barshad I. (1955) Adsorptive and swelling properties of clay-water system. *Clays Clay Technol. Bull.* **169,** 70–77.

Basu S. and Sharma M. M. (1994) Effect of dielectric saturation on disjoining pressure in thin films of aqueous electrolytes. *J. Colloid Interface Sci.* **165,** 355–366.

Benavente D., García del Cura M. A., García-Guinea J., Sánchez-Moral S., and Ordóñez S. (2004) Role of pore structure in salt crystallisation in unsaturated porous stone. *J. Cryst. Growth* **260,** 532–544.

Blowes D. W., Reardon J. E., Jambor J. L., and Cherry J. A. (1991) The formation and potential importance of cemented layers in inactive sulfide mine tailings. *Geochim. Cosmochim. Acta* **55,** 965–978.

Borek S. L. (1994) Effect of humidity on pyrite oxydation. In *Environmental Geochemistry of Sulfide Oxidation* (eds. C. N. Alpers and D. W. Blowes), pp. 31–44. ACS Symposium Series 550. American Chemical Society.

Bourrié G., Tessier D., and Pedro G. (1983) Considérations sur les phénomènes d'altération dans les systèmes à eau liée ($a_w < 1$). *Sci. Géol., Mém.* **71,** 25–33.

Boyarskii D. A., Tikhonov V. V., and Komarova N. Y. (2002) Model of dielectric constant of bound water in soil for applications of microwave remote sensing. *Progress In Electromagn. Res.* **35,** 251–269.

Bruton C. J. and Viani B. E. (1992) Geochemical modeling of water–rock interactions in the unsaturated zone. In *Proceedings of the 1992 Water-Rock Interaction* (eds. Y. K. Kharaka and A. S. Maest), pp. 705–708. Balkema, Rotterdam.

Byrne R. H. and Laurie S. H. (1999) Influence of pressure on chemical equilibria in aqueous systems—With particular reference to seawater. *Pure Appl. Chem.* **71,** 971–890.

Chivot J. (2004) Thermodynamique des produits de corrosion. Fonctions thermodynamiques de solubilité, diagrammes Eh-pH des systèmes Fe-H_2O, Fe-CO_2-H_2O, Fe-S-H_2O, Cr-H_2O et Ni-H_2O en

fonction de la température. Document ANDRA, Collection Sciences et Techniques.

Clegg S. L. and Whitfield M. (1991) Activity coefficients in natural waters. In *Activity Coefficients in Electrolyte Solution,* 2nd ed. (ed. K. S. Pitzer), pp. 279–434. CRC Press.

Davies C. W. (1962) *Ion Association.* Butterworths, London.

Debye P. and Hückel E. (1923) Zur theorie der electrolytes I. *Phys. Z.* **24,** 185–193.

Derjaguin B. V., Churaev N. V., and Muller V. M. (1987) *Surface Forces.* Plenum, New York.

Fennemore G. G., Neller W. C., and Davis A. (1998) Modeling pyrite oxidation in arid environments. *Environ. Sci. Technol.* **32,** 2680–2687.

Fernández D. P., Goodwin A. R. H., Lemmon E. W., Levelt Sengers J. M. H., and Williams R. C. (1997) A formulation for the static permittivity of water and steam at temperatures from 238 K to 873 K at pressures up to 1200 MPa, including derivatives and Debye-Hückel coefficients. *J. Phys. Chem. Ref. Data* **26,** 1125–1166.

Gooddy D. C., Clay J. W., and Bottrell S. H. (2002) Redox-driven changes in porewater chemistry in the unsaturated zone of the chalk aquifer beneath unlined cattle slurry lagoons. *Appl. Geochem.* **17,** 903–921.

Green J. L., Durben D. J., Wolf G. H., and Angell C. A. (1990) Water and solutions at negative pressure: Raman spectroscopic study to −80 megapascals. *Science* **249,** 649–652.

Guevremont J. M., Elsetinow A. R., Strongin D. R., Bebie J., and Schoonen M. A. A. (1998) Structure sensitivity of pyrite oxidation: Comparison of the (100) and (111) planes. *Am. Mineral.* **83,** 1353–1356.

Hecht H. and Kölling M. (2002) Investigation of pyrite-weathering processes in the vadose zone using optical oxygen sensors. *Environ. Geol.* **42,** 800–809.

Helgeson H. C. (1969) Thermodynamics of hydrothermal systems at elevated temperatures and pressures. *Am. J. Sci.* **267,** 729–804.

Helgeson H. C. and Kirkham D. H. (1974) Theoretical prediction of the thermodynamic behavior of aqueous electrolytes at high pressures and temperatures: II. Debye-Hückel parameters for activity coefficients and relative partial molal properties. *Am. J. Sci.* **274,** 1199–1261.

Helgeson H. C., Delany J. M., Nesbitt H. W., and Bird D. K. (1978) Summary and critique of the thermodynamic properties of rock-forming minerals. *Am. J. Sci.* **278-A**, 1–229.

Helgeson H. C., Kirkham D. H., and Flowers G. C. (1981) Theoretical prediction of the thermodynamic behavior of aqueous electrolytes at high pressures and temperatures: IV. Calculation of activity coefficients, osmotic coefficients, and apparent molal and standard and relative partial molal properties to 600°C and 5 kb. *Am. J. Sci.* **281,** 1249–1516.

Hernandez A. J., Adarve M. J., Gil A., and Pastor J. (1999) Soil salination from landfill leachates: Effects on the macronutrient content and plant growth of four grassland species. *Chemosphere* **38,** 1693–1711.

Hillel D. (1998) *Environmental Soil Physics.* Academic Press, New York.

Hollings P., Hendry M. J., Nicholson R. V., and Kirkland R. A. (2001) Quantification of oxygen consumption and sulphate release rates for waste rock piles using kinetic cells: Cluff lake uranium mine, northern Saskatchewan, Canada. *Appl. Geochem.* **16,** 1215–1230.

IAPWS (1994) *IAPWS Release on Surface Tension of Ordinary Water Substance.* IAPWS.

Jambor J. L. and Blowes D. W. (1998) Theory and application of mineralogy in environmental studies of sulfide-bearing mine wastes. In *Modern Approaches to Ore and Environmental Mineralogy* (eds. L. J. Cabri and D. J. Vaughan), pp. 367–401. Mineralogical Association of Canada.

Jerz J. K. and Rimstidt J. D. (2004) Pyrite oxidation in moist air. *Geochim. Cosmochim. Acta* **68,** 701–714.

Johnson J. W., Oelkers E. H., and Helgeson H. C. (1992) SUPCRT92: A software package for calculating the standard molal thermodynamic properties of minerals, gases, and aqueous species from 1 to 5000 bars and 0° to 1000°C. *Comp. Geosci.* **18,** 899–947.

Kehiaian H. V. (1997) Virial coefficients of selected gases. In *CRC Handbook of Chemistry and Physics,* 78th ed., 1997-1998 (ed. D. R. Lide), pp. 6-23–6-42. CRC Press, Boca Raton, FL.

Lassin A., Pinault J.-L., and Azaroual M. (2003) Thermodynamique de la zone non saturée en eau des systèmes géologiques: II. Elaboration d'un code de calcul spécifique. BRGM Report. BRGM/RP-52010-FR.

Lassin A., Azaroual M., Pinault J.-L., Amraoui N. and Mercury L. (2004) Solubility of gases and minerals in soil waters: Thermodynamic calculations. In *Proceedings of the 8th International Meeting on Soils with Mediterranean Type of Climate* (eds. R. Bouabid, M. Badraoui, and M. Bamouh), pp. 29–32. Moroccan Association of Soil Sciences (AMSSOL).

Manciu M. and Ruckenstein E. (2003) Specific ion effects via ion hydration: I. Surface tension. *Adv. Colloid Interf. Sci.* **105,** 63–101.

Mercury L. and Tardy Y. (1997a) Negative pressure and thermodynamic properties of capillary water. A concise review paper. *C. R. Acad. Sci. Paris* **324,** *11,* 863–873.

Mercury L. and Tardy Y. (1997b) Physicochemical features of water in capillaries and fog water droplets. *C. R. Acad. Sci. Paris* **325,** *12,* 947–954.

Mercury L. and Tardy Y. (2001) Negative pressure of stretched liquid water. Geochemistry of soil capillaries. *Geochim. Cosmochim. Acta* **65,** 3391–3408.

Mercury L., Azaroual M., Zeyen H., and Tardy Y. (2003) Thermodynamic properties of solutions in metastable systems under negative or positive pressures. *Geochim. Cosmochim. Acta* **67,** 1769–1785.

Mercury L., Pinti D. L., and Zeyen H. (2004) The effect of the negative pressure of capillary water on atmospheric noble gas solubility in ground water and palaeotemperature reconstruction. *Earth Planet. Sci. Lett.* **223,** 147–161.

Mercury L. and Tardy Y. (2004) Response to the Comment by J. V. Walther on "Negative pressure of stretched liquid water: Geochemistry of soil capillaries" (2001), *Geochim. Cosmochim. Acta* **65,** 3391–3408; and "Thermodynamic properties of solutions in metastable systems under negative or positive pressures" (2003), *Geochim. Cosmochim. Acta* **67,** 1769–1785. *Geochim. Cosmochim. Acta* **68**, 2775–2780.

Mulyanto B. and Stoops G. (2003) Mineral neoformation in pore spaces during alteration and weathering of andesitic rocks in humid tropical Indonesia. *Catena* **54,** 385–391.

Michard G. (1989) *Equilibres chimiques dans les eaux naturelles.* Publisud, Orsay.

Naumov G. B., Ryzhenko B. N., and Khodakovsky I. L. (1974) Handbook of thermodynamic data. English edition translated from Russian by USGS. Report USGS-WRD-74-001. Distributed by NTIS, U.S. Department of Commerce.

Nordstrom D. K. and Alpers C. N. (1999) Negative pH, efflorescent mineralogy, and consequences for environmental restoration at the Iron Mountain Superfund site, California. *PNAS* **96,** 3455–3462.

Parkhurst D. L. and Appelo C. A. J. (1999) User's guide to PHREEQC (version 2)—A computer program for speciation, batch-reaction, one-dimensional transport, and inverse geochemical calculation. Report 99-4259. U.S. Geological Survey, Water-Resources Investigations.

Pitzer K. S. (1973) Thermodynamics of electrolytes—I. Theoretical basis and general equations. *J. Phys. Chem.* **77,** 268–277.

Pitzer K. S. (1995) Ionic fluids: Near-critical and related properties. *J. Phys. Chem.* **99,** 13070–13077.

Prigogine I. and Defay R. (1950) *Traité de thermodynamique. Tomes I et II: Thermodynamique chimique.* Desoer, Brussels.

Robie R. A. and Hemingway B. S. (1995) Thermodynamic properties of minerals and related substances at 298.15 K and 1 bar (10^5 Pascals) pressure and at higher temperatures. U.S. Geol. Bull. 2131.

Ruckenstein E. and Manciu M. (2003) Specific ion effects via ion hydration: II. Double layer interaction. *Adv. Colloid Interf. Sci.* **105,** 177–200.

Seyfried M. S. and Murdock M. D. (2004) Measurement of soil water content with a 50-MHz soil dielectric sensor. *Soil Sci. Soc. Am. J.* **68,** 394–403.

Shock E. L. and Helgeson H. C. (1988) Calculation of the thermodynamic and transport properties of aqueous species at high pressures and temperatures: Correlation algorithms for ionic species and equation of state predictions to 5 kb and 1000°C. *Geochim. Cosmochim. Acta* **52,** 2009–2036.

Shock E. L., Helgeson H. C., and Sverjensky D. A. (1989) Calculation of the thermodynamic and transport properties of aqueous species at high pressures and temperatures: Standard partial molal properties of inorganic neutral species. *Geochim. Cosmochim. Acta* **53,** 2157–2183.

Shock E. L., Oelkers E. H., Johnson J. W., Sverjensky D. A., and Helgeson H. C. (1997) Inorganic species in geologic fluids: Correlations among standard molar thermodynamic properties of aque-

ous cations, oxyanions, acid oxyanions, oxyacids and hydroxide complexes. *Geochim. Cosmochim. Acta* **61,** 907–950.
Span R. and Wagner W. (2000) Das Software-Grundpaket zur Berechnung thermodynamischer Daten in Referenzqualität. Ruhr-Universität Bochum Report.
Tanger J. C. IV and Helgeson H. C. (1988) Calculation of the thermodynamic and transport properties of aqueous species at high pressures and temperatures: Revised equations of state for the standard partial molal properties of ions and electrolytes. *Am. J. Sci.* **288,** 19–98.
Tardy Y. (1982) Kaolinite and smectite stability in weathering conditions. In *Crystal Growth Processes in Sedimentary Environments* (eds. R. Rodriguez and I. Sunagawa), Estudios Geologicos, Vol. 38, pp. 295–312. International Mineralogical Association.
Tardy Y. and Nahon D. (1985) Geochemistry of laterites, stability of Al-goethite, Al-hematite, and Fe^{3+}-kaolinite in bauxites and ferricretes: An approach to the mechanism of concretion formation. *Am. J. Sci.* **285,** 865–903.
Tardy Y. and Novikoff A. (1988) Activité de l'eau et déplacement des équilibres gibbsite–kaolinite dans les profils latéritiques. *C. R. Acad. Sci., Paris Ser. 2,* **306,** 39–44.
Todd E. C., Sherman D. M., and Purton J. A. (2003) Surface oxidation of pyrite under ambient atmospheric and aqueous (pH = 2 to 10) conditions: Electronic structure and mineralogy from X-ray absorption spectroscopy. *Geochim. Cosmochim. Acta* **67,** 881–893.
Trolard F. and Tardy Y. (1987) The stabilities of gibbsite, boehmite, aluminous goethites and aluminous hematites in bauxites, ferricretes and laterites as a function of water activity, temperature and particle size. *Geochim. Cosmochim. Acta* **51,** 945–957.
Trolard F. and Tardy Y. (1989) A model of Fe^{3+}-kaolinite, Al^{3+}-goethite, Al^{3+}-hematite equilibria in laterites. *Clay Min.* **24,** 1–21.
Verdes G. and Gout R. (1987) Réhydratation d'oxydes d'aluminium amorphes. Application à l'étude de l'équilibre boehmite–bayérite. *Bull. Minéral.* **110,** 579–587.
Wagman D. D., Evans W. H., Parker V. B., Schumm R. H., Halow I., Bailey S. M., Churney K. L., and Nutall R. L. (1982) The NBS tables of chemical thermodynamic properties. *J. Phys. Chem. Ref. Data* **11** (Suppl. 2), 1–391.
Wagner W. and Pruss A. (2002) The IAPWS formulation 1995 for the thermodynamic properties of ordinary substance for general and scientific use. *J. Phys. Chem. Ref. Data* **31,** 387–535.
Wasserman E., Wood B., and Davies A. (1995) Equation of state for aqueous silica species at pressures from 1 bar to 20 kbar and temperatures from 25° to 900°C based on simulated values of dielectric constant. *Chem. Geol.* **121,** 3–9.
Zheng Q., Durben D. J., Wolf G. H., and Angell C. A. (1991) Liquids at large negative pressures: Water at the homogeneous nucleation limit. *Science* **254,** 829–832.
Zilberbrand M. (1997) A nonelectrical mechanism of ion exclusion in thin water films in finely dispersed media. *J. Colloid Interface Sci.* **192,** 471–474.
Zilberbrand M. (1999) On equilibrium constants for aqueous geochemical reactions in water unsaturated soils and sediments. *Aquat. Geochem.* **5,** 195–206.

APPENDIX

Calculation of the Fugacity Coefficients of the Main Atmospheric Gases (O_2, CO_2, H_2O)

For each gas, the fugacity may be calculated if the second virial coefficient B is known. The coefficients corresponding to each of the main reactive gases of the atmosphere (O_2 and CO_2), as well as its major constituent (N_2) are given in Table A-1. According to Prigogine and Defay (1950), the fugacity coefficient $\Phi(T,p)$ of a real pure gas is given, as a first approximation, by:

$$\Phi(T,p) = f/p = \exp(Bp/RT). \quad \text{(A-1)}$$

If one considers a binary mixture consisting of gases 1 and 2, the respective fugacity coefficients are given by the following equations:

Table A-1. Second virial coefficients B of the gases O_2, CO_2 and N_2, at 25°C, according to Kehiaian (1997).

Gas	N_2	O_2	CO_2
$B \times 10^6$ ($m^3 \cdot mol^{-1}$)	−4	−16	−127

$$\Phi_1(T,p) = \frac{\exp\left[\ln\left(N_1 RT/v\right) + 2\times(B_{11}N_1 + B_{12}N_2)\right]}{v}, \quad \text{(A-2)}$$

and

$$\Phi_2(T,p) = \frac{\exp\left[\ln\left(N_2 RT/v\right) + 2\times(B_{12}N_1 + B_{22}N_2)\right]}{v}, \quad \text{(A-3)}$$

where

$$v = \frac{RT}{p} \times \left(1 + \frac{p}{RT}(B_{11}N_1^2 + 2B_{12}N_1N_2 + B_{22}N_2^2)\right). \quad \text{(A-4)}$$

N_i is the mole fraction of the gas i (i = 1, 2); v is the molar volume of the gaseous mixture; B_{ii} is the second virial coefficient of the gas i, stemming from the mutual interaction of the molecules of the constituent i; B_{12} corresponds to the interaction of molecules 1 with molecules 2; p is the total pressure of the gaseous phase, the partial pressures being equal to $N_i \times p$.

If gases 1 and 2 have similar molecular structures, B_{12} may be estimated by (Prigogine and Defay, 1950):

$$B_{12} \approx (B_{11} + B_{22})/2. \quad \text{(A-5)}$$

The application of the relation (A-1) to the pure gases O_2 and CO_2 makes it possible to evaluate their fugacity coefficient as a function of the pressure, arbitrarily taken between 10^{-3} and 100 MPa for the illustration shown in Figure A-1. The application of the relations A-1 to A-5 to the binary mixture (N_2, O_2), with respective proportions of 78% and 21%, makes it possible to evaluate the fugacity coefficient of oxygen in the air. Then, by considering the air as a unique constituent, the same relations make it possible to evaluate, as a function of the pressure, the fugacity coefficient of the CO_2, which represents 0.033% of the binary mixture (air, CO_2). The results obtained are detailed in Figure A-1 and show that the fugacity coefficients of the gases considered deviate in a significant manner from the value 1 for higher pressures or around 0.5 MPa as regards CO_2, and greater than or around 1 MPa as regards O_2, whether the gases are pure or in the air. Beyond these pressures, the fugacity of the gases deviates from their partial pressure.

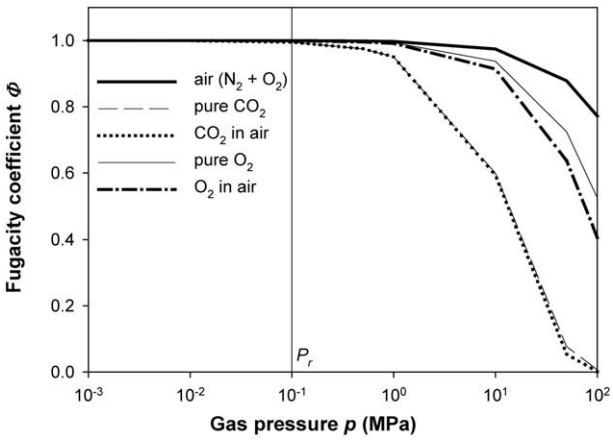

Fig. A-1. Fugacity coefficients of atmospheric gases (pure and in air) as a function of pressure, at T = 25°C.